Self focusing in a spatially modulated electrostatic field particle accelerator

F. Russman, S. Marini, E. Peter, G. I. de Oliveira, and F. B. Rizzato

Citation: Physics of Plasmas **25**, 023110 (2018); doi: 10.1063/1.5020724
View online: https://doi.org/10.1063/1.5020724
View Table of Contents: http://aip.scitation.org/toc/php/25/2
Published by the American Institute of Physics

Self focusing in a spatially modulated electrostatic field particle accelerator

F. Russman,[1,a)] S. Marini,[2,b)] E. Peter,[1,c)] G. I. de Oliveira,[3,d)] and F. B. Rizzato[1,e)]
[1]*Instituto de Física, Universidade Federal do Rio Grande do Sul, Caixa Postal 15051, 91501-970 Porto Alegre, RS, Brazil*
[2]*LULI, Sorbonne Université, CNRS, École Polytechnique, CEA, Université Paris-Saclay, F-75252 Paris cedex 05, France*
[3]*Instituto de Física, Universidade Federal do Mato Grosso do Sul, Caixa Postal 549, 79070-900 Campo Grande, MS, Brazil*

(Received 26 December 2017; accepted 8 February 2018; published online 22 February 2018)

In the present analysis, we study the action of a three-dimensional (3*D*) modulated electrostatic wave over a charged particle. Meanwhile, the particle's velocity is smaller than the phase-velocity of the carrier, and the particle could be reflected by the potential or could pass through the potential with no significant change in the longitudinal velocity—and its dynamics could be described by a ponderomotive approximation. Otherwise, the particle is trapped by the potential and it is accelerated towards the speed of light, independently of the initial particle's phase—in this case, the ponderomotive approximation is no longer valid. During the acceleration process, numerical simulations show the particle is focused, simultaneously. These results suggest the accelerator proposed here is promising. *Published by AIP Publishing.* https://doi.org/10.1063/1.5020724

I. INTRODUCTION

Charged particle accelerators need some optimum length to accelerate beams to the desired final velocities. In the case of the electrostatic accelerators such as the accelerators of the pioneers Cockcroft-Walton[1] and Van de Graaff,[2] the mentioned length is the distance between electrodes. In electromagnetic accelerators,[3] on the other hand, the optimum length is dictated either by the size of accelerating cells in radio-frequency (RF)[4,5] or by the distance covered by accelerating particles trapped in the wakefields of plasma based accelerators, for instance.[6]

Along the accelerator length, particles need to stay close to the axis of the device where fields are more intense and where acceleration is coherently driven, a fact that poses some issues since space charge or transverse ponderomotive effects naturally push particles outwards. Magnetic focusing is commonly used to keep the beam close to the transport axis in RF systems,[7–10] while their own wakefields may trap particles close to the axis in plasma based accelerators.

We discuss yet an alternative approach that results from trapping particles in the accelerating wave through a slowly modulated electrostatic wave, after an initial ponderomotive phase brings particle up to resonant conditions. The mechanism is basically a three-dimensional extension of the previous one-dimensional model recently studied.[11] Differently of the beat wave accelerator, for example Refs. 7, 12, and 13, which could provide high field intensities,[14,15] on that one-dimensional model, the acceleration does not depend on the initial phase of the particle. The longitudinal modulation of the electrostatic wave is preserved in comparison with the previous work,[11] and the transverse dynamics of the system and the transverse profile of the wave are also taken into account. The ponderomotive approximation[16,17] is applied, eliminating the high frequency terms associated with the longitudinal coordinate. The approximation reasonably describes the mean value of the particle's dynamics when the system is far from the resonance.

Three different regimes are observed: the reflecting regime, where the particle is reflected by the electrostatic wave; the passing regime, in which the particle passes through the wave and does not experience substantial acceleration; and, finally, the accelerating regime. In the accelerating regime, the longitudinal velocity of the particle becomes greater than the phase-velocity of the carrier. At this moment, the particle is trapped by the potential and it is accelerated towards c (speed of light). Simultaneously, under proper conditions, the radial coordinate of the particle decreases. The accelerating and the focusing behaviours together are highly interesting from the point of view of particle accelerators and beam transport.

This paper is organized as follows: in Sec. II, we present the 3*D* model and the ponderomotive approximation as well; in Sec. III, we show the main results, the role of each parameter of the model, and the details of each regime; and, finally, in Sec. IV we draw our conclusions.

II. THE 3D MODEL

A. Full model

The three-dimensional model used in this work is a multidimensional extension of Ref. 11, where we add transverse profiles for the field and particle dynamics. In this case, the electrostatic modulated wave has also a radial profile. The Lagrangian that describes the interaction of a relativistic particle with the electrostatic modulated wave is thus expressed as

[a)]russman@ufrgs.br
[b)]marini@ufrgs.br
[c)]peterpeter@uol.com.br
[d)]glaucius.oliveira@ufms.br
[e)]rizzato@if.ufrgs.br

$$L = -mc^2\sqrt{1 - \frac{\dot{r}^2 + r^2\dot{\theta}^2 + \dot{z}^2}{c^2}} - q\varphi(z, r, t), \qquad (1)$$

where c is the speed of light, φ is the electrostatic modulated wave, and m and q are the mass and the charge of the electron, respectively.

The electrostatic modulated wave is written as

$$\varphi(z, r, t) = \varphi_0 \exp\left(-\frac{z^2}{\sigma_z^2} - \frac{r^2}{\sigma_r^2}\right)\cos(kz - \omega t), \qquad (2)$$

where the amplitude φ_0 is constant, k and ω are the wavevector and the frequency of a carrier moving along the z axis, and σ_z and σ_r measure the envelope length and the radial profile length of the wave, respectively. We consider $\sigma_z, \sigma_r \gg 1/k$ to enforce the condition of a slowly modulated wave train. The physics of this purely electrostatic modulated wave proposed here is similar to the physics of a particle submitted to the combined action of collinear electromagnetic and wiggler fields. This kind of arrangement is usually seen in inverse free-electron lasers devices.[18–20]

A dimensionless Hamiltonian can be obtained from the Lagrangian of Eq. (1) by normalizing z by k^{-1} and t by ω^{-1}

$$H(r, p_r, p_\theta, z, p_z, t) = \gamma + \varphi_0 \exp\left(-\frac{z^2}{\sigma_z^2} - \frac{r^2}{\sigma_r^2}\right)\cos(z - t). \qquad (3)$$

The relativistic factor $\gamma = \sqrt{[1 + (p_r^2 + p_\theta^2/r^2 + p_z^2)/\alpha]}$ is written in terms of the dimensionless momenta p_r, p_θ^2/r^2, and p_z^2, with $\alpha = v_\phi^2/c^2$ and $v_\phi = \omega/k$ as the phase-velocity of the carrier. The Hamiltonian H is normalized by the factor mc^2 and φ_0 is normalized by the factor mc^2/q.

Hamiltonian canonical equations for this problem yield

$$\begin{aligned}
\dot{p}_z &= \varphi_0 \exp\left(-\frac{z^2}{\sigma_z^2} - \frac{r^2}{\sigma_r^2}\right)\left[\frac{2z}{\sigma_z^2}\cos(z - t) + \sin(z - t)\right],\\
\dot{p}_r &= \frac{p_\theta^2}{\alpha\gamma r^3} + \frac{2r}{\sigma_r^2}\varphi_0 \exp\left(-\frac{z^2}{\sigma_z^2} - \frac{r^2}{\sigma_r^2}\right)\cos(z - t),\\
\dot{p}_\theta &= 0,\\
\dot{z} &= \frac{p_z}{\gamma\alpha},\\
\dot{r} &= \frac{p_r}{\gamma\alpha},\\
\dot{\theta} &= \frac{p_\theta}{r^2\gamma\alpha}.
\end{aligned} \qquad (4)$$

As can be seen, p_θ is a constant of motion because the problem has symmetry in θ coordinate. Moreover, $\dot{p}_r$ may be negative, which allows decreasing values of r and concomitant particle focusing near the transport axis during the system dynamics. For that, the relation $\cos(z - t) < -(p_\theta {\sigma_r}^2/2\alpha\gamma r^4)[\varphi_0 \exp(-z^2/{\sigma_z}^2 - r^2/{\sigma_r}^2)]^{-1}$ must be satisfied: as $(p_\theta {\sigma_r}^2/2r\alpha\gamma r^4)[\varphi_0 \exp(-z^2/{\sigma_z}^2 - r^2/{\sigma_r}^2)]^{-1}$ is positive, the term $\cos(z - t)$ must be negative and greater in modulus than that term. The focusing (the decrease in r), as already written, is a very important and desirable feature for beam transportation.

In all the cases discussed in this work, we use $\dot{r}(t = 0) = 0$ and $\ddot{r}(t = 0) = 0$, the latter condition obtained by a convenient choice of p_θ. Under these conditions, the system starts from equilibrium, without initial force and velocity in radial coordinate.

B. Ponderomotive approximation

Despite the complicated relation between p_r, p_z, and p_θ present in γ, if the initial conditions are such that the particle's dynamics is far from resonance (i.e., the maximum longitudinal velocity of the particle is smaller than the phase-velocity of the carrier), the ponderomotive approximation describes (through a self-consistent set of time averaged low-frequency variables[21]) in a reasonable way the evolution of the particle, both in the reflecting regime (negative final longitudinal velocity) or in the passing regime (positive final longitudinal velocity). Moreover, the accuracy of the approximation is better as we increase the gap of the maximum value of longitudinal particle's velocity and the resonance velocity.

The ponderomotive approximation removes the high-frequency jitter induced by the oscillatory character of the carrier and allows to describe the dynamics solely in terms of time-averaged quantities.

In our case, to build the ponderomotive approximation, a change in the momentum p_z is made: $p_z = P_z + \partial f/\partial z$ (where P_z is a low frequency variable that describes the mean value during the evolution of p_z—the mean of p_z from the full model is obtained executing a time average over a moving window). A change in z is also necessary in order to obtain a canonical transformation ($Z = z + \partial f/\partial P_z$). However, as $\varphi/\sigma_z \ll 1$, which is similar to $(Z - z)/\sigma_z \ll 1$, z and Z are approximately the same. The generating function f is such that f absorbs the high-frequency terms, giving to the new momentum (P_z) a status of a low-frequency variable and it is written, in first-order, as

$$f = \frac{\varphi_0}{\left[1 - \frac{P_z}{\alpha\Gamma}\right]} e^{-z^2/{\sigma_z}^2} e^{-r^2/{\sigma_r}^2} \sin(z - t), \qquad (5)$$

where $\Gamma = \sqrt{1 + [(p_r^2 + p_\theta^2/r^2 + P_z^2)/\alpha]}$.

Executing the adequate substitutions, the ponderomotive Hamiltonian, $\mathcal{H}$, obtained is expressed as

$$\mathcal{H} = \Gamma + \frac{1}{4\alpha\Gamma}\frac{{\varphi_0}^2 e^{-2Z^2/{\sigma_z}^2} e^{-2r^2/{\sigma_r}^2}}{(P_z/\alpha\Gamma - 1)^2}\left(1 - \frac{{P_z}^2}{\alpha\Gamma^2}\right), \qquad (6)$$

where the capital Z represent the change position variable. That can be understood as the position of the particle's oscillation center and obtained through the generating function f as $Z = z + \partial f/\partial P_z$. Through the ponderomotive Hamiltonian, the mean value of p_z could be calculated by the relation $p_z = P_z$. As one has p_z, $v_z = p_z/\alpha\gamma(p_z)$. Equation (6) could provide the envelope of v_z: $v_{z_{min/max}} = p_{z_{min/max}}/\alpha\gamma$, where $p_{z_{min}} = P_z + min(\partial f/\partial z)$ and $p_{z_{max}} = P_z + max(\partial f/\partial z)$.

III. RESULTS

As commented earlier, the present system has some similarities with the one dimensional model proposed in Ref. 11, so we use the techniques employed in this previous work. In order to find an accelerating regime, we expressed the final longitudinal velocities of the particles as a colour graded map: variables φ_0, σ_r, σ_z, and α were maintained fixed, while $r_0 = r(t=0)$ and $v_{z0} = v_z(t=0)$ were varied. The result is shown in Fig. 1. The map was built for $\alpha^{1/2} = 0.90$, $\varphi_0 = 1$, $\sigma_r = 50$, and $\sigma_z = 100$. Additionally, $\dot{r}(t=0) = \ddot{r}(t=0) = 0$. As can be seen, there are three distinct regions (exactly as in Ref. 11): The blue color represents negative final velocities; the white, gray, and black colors indicate positive velocities without significant acceleration; and, finally, the red and yellow colors show the region where the particle is accelerated (up to $0.997c$) by the electrostatic field. The points labelled in the map are explored in details later on.

In general, if r_0 increases, the initial longitudinal velocity needed to achieve the same final velocity also increases. This is explained when one looks at Eq. (2): The transverse profile of the wave is such that the intensity decays with r. Then, to increase r_0 is similar to reduce φ_0. As in Ref. 11, there is a periodic array of less-than-effective curves inside the accelerating region. The meaning of these singular curves is the same: Their vertices correspond to the fixed points of the dynamics where injecting and exiting velocities are identical.

The point 2 of Fig. 1 represents the reflecting regime of this system and is shown in details in Fig. 2. Panel (a) depicts the time evolution of the longitudinal velocity, v_z (in $\alpha^{-1/2}$ units, which is equal to the velocity normalized to the speed of light), denoted by the red solid line and the time evolution of the radial velocity, v_r (in $\alpha^{-1/2}$ units), described by the blue solid line. The resonant velocity is given by the green solid line, while the mean values of v_r and v_z given by the ponderomotive approximation are expressed by the black dashed lines (the gray solid line is from the integration of Eq. (4) and express the mean of v_z evaluated through a moving window). The ponderomotive approximation well describes the evolution of the mean of the velocities, offering

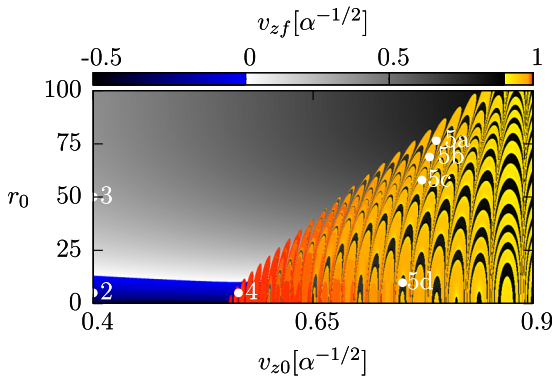

FIG. 1. Color graded map of the longitudinal exiting velocities for $\alpha^{1/2} = 0.90$, $\varphi_0 = 1$, $\sigma_r = 50$, and $\sigma_z = 100$. In the horizontal axis is represented the initial longitudinal velocity of the particle, v_{z0}, while in the vertical axis is expressed the initial radial coordinate of the particle, r_0. The points labeled in the map are discussed later on.

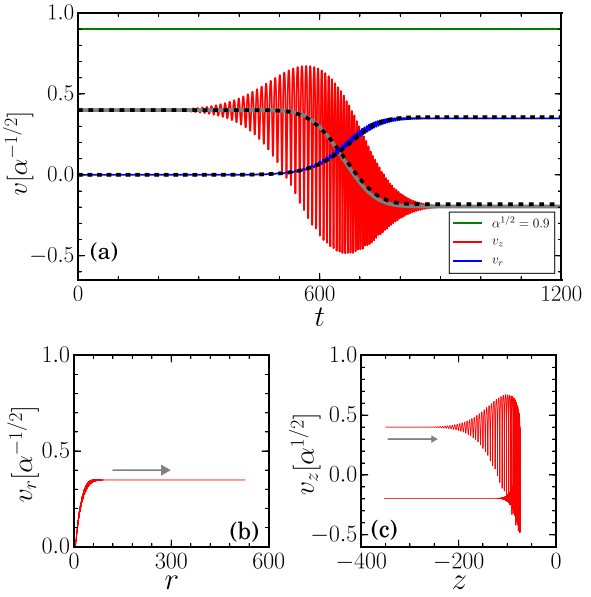

FIG. 2. Respective time evolutions for v_z and v_r are shown in panel (a) (dashed line is from the ponderomotive approximation). Panel (b) is for the phase-space in r-coordinate, while panel (c) is for the phase-space in z-coordinate. The results were plotted for $\sqrt{\alpha} = 0.9$, $\varphi_0 = 1.0$, $\sigma_z = 100$, $\sigma_r = 50$, $r(t=0) = 5$, and $v_z(t=0)[\alpha^{-1/2}] = 0.4$. This set of parameters is represented by the label 2 in Fig. 1.

a good estimative of the final v_z and v_r. The particle begins its dynamics with $\dot{r}(t=0) = 0$ and $\dot{v}_z(t=0) \approx 0$, but as the effect of the electrostatic field becomes relevant, the radial velocity grows, in a way that the final radial velocity is about $0.36c$. On the other hand, the longitudinal velocity oscillates when the effect of the electrostatic field becomes relevant and then the particle is reflected by the field. The final longitudinal velocity of the particle is $v_z[\alpha^{-1/2}] \approx -0.18$. In panel (b), a phase-space v_r *vs.* r is shown. Initially, $\dot{r}(t=0) = \ddot{r}(t=0) = 0$ and $r(t=0) = 5$, then, as we see in panel (a), the radius and the radial velocity grow. Due to the longitudinal modulation of the electrostatic field, when $|z| \gg \sigma_z$, the action of the field is negligible and the system acquires its final velocities. Finally, in panel (c) is plotted the phase-space v_z *vs.* z. The particle oscillates while getting closer of the center of the longitudinal electrostatic field shape and then it is reflected.

Particle could also pass through the field in a way that it does not experience any appreciable change between its initial and its final velocities—this is the passing regime. To describe the evolution of the passing regime, we explore in details the point 3 of Fig. 1. Figure 3 was built for $\varphi_0 = 1.0$, $\sigma_z = 100$, $\sigma_r = 50$, $r(t=0) = 50$, and $v_z(t=0)[\alpha^{-1/2}] = 0.4$. Panel (a) of Fig. 3 shows the evolution of the longitudinal and radial velocities. The longitudinal velocity starts from $v_z(t=0)[\alpha^{-1/2}] = 0.4$, then it oscillates due to the electrostatic field and reaches its final value ($v_z[\alpha^{-1/2}] \approx 0.32$). The radial velocity, which is initially zero, grows to $v_r[\alpha^{-1/2}] \approx 0.24$. The dashed lines represent the mean values of the velocities v_z and v_r, integrated from the ponderomotive approximation and the gray solid line is from Eq. (4). As the system is far from the resonance, the approximation works well, except in the region near $z = 0$. The phase-space v_r *vs.* r

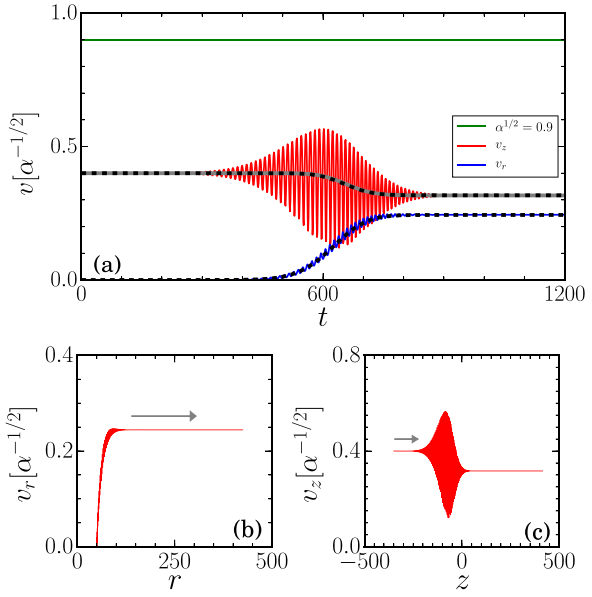

FIG. 3. Respective time evolutions for v_z and v_r are shown in panel (a) (dashed line is from the ponderomotive approximation). Panel (b) is for the phase-space in r-coordinate, while panel (c) is for the phase-space in z-coordinate. The results were plotted for $\sqrt{\alpha}=0.9$, $\varphi_0=1.0$, $\sigma_z=100$, $\sigma_r=50$, $r(t=0)=50$, and $v_z(t=0)[\alpha^{-1/2}]=0.4$. This set of parameters is represented by the label 3 in Fig. 1.

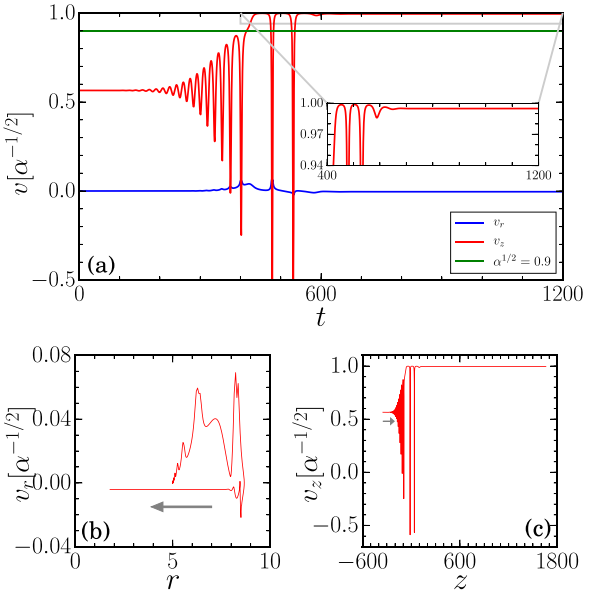

FIG. 4. Respective time evolutions for v_z and v_r are shown in panel (a). Panel (b) is for the phase-space in r-coordinate, while panel (c) is for the phase-space in z-coordinate. The results were plotted for $\sqrt{\alpha}=0.9$, $\varphi_0=1.0$, $\sigma_z=100$, $\sigma_r=50$, $r(t=0)=5$, and $v_z(t=0)[\alpha^{-1/2}]=0.57$. This set of parameters is represented by the label 4 in Fig. 1.

is plotted in panel (b). The radial velocity grows along the system dynamics, which implies that the radius also grows: There is no focusing of the beam. In panel (c), the phase-space v_z *vs.* z is presented. As the maximum velocity of the particle is under the resonant velocity, the particle is not trapped by the electrostatic field and is not accelerated. The final longitudinal velocity of the particle is slightly smaller than the initial longitudinal velocity. It may be explained due the change in the radial velocity—kinetic energy of the particle was transferred from the longitudinal to the radial coordinates during the dynamics.

So far as acceleration is concerned, the most efficient regime in the present model, which is denoted by the point 4 in Fig. 1, is shown in detail in Fig. 4 for $r(t=0)=5$ and $v_z(t=0)[\alpha^{-1/2}]=0.57$. The evolution of the longitudinal (red solid line) and the radial (blue solid line) velocities is depicted in panel (a). As can be seen, the red solid line intercepts the green line (resonant velocity) and then the particle is accelerated towards c around the maximum of the potential well. Exactly as in Ref. 11, the particle is accelerated and it is not pushed back by the next potential maximum because the value of the amplitude of the potential well decays as $|z|$ is increased. It can be seen that when the particle is trapped and accelerated by the potential well, the relation $\dot{r}<0$ is satisfied $(\cos(z-t)<-(p_\theta{\sigma_r}^2/2\alpha\gamma r^4)[\varphi_0\exp(-z^2/{\sigma_z}^2-r^2/{\sigma_r}^2)]^{-1})$. It could be understood as an effect of focusing, where the radial coordinate of the particle decreases, as seen in the phase-space v_r *vs.* r on panel (b) of Fig. 4. But not always the particle goes to $r\approx 0$ while it is accelerated. There are some cases where $\dot{r}>0$ just before the trapping that even $\dot{r}$ assuming negative values during the trapping, and it is not enough to reduce $r(t)$ to smaller values than r_0. The phase-space v_z against z is denoted in panel (c): The particle is accelerated near the center (around $z=0$) of the longitudinal modulation of the electrostatic wave.

Inside the accelerating regime, there is a series of curves that resemble half moons. The vertices of these curves are similar to "fixed points" of the dynamics of the particles: The injecting and the exiting longitudinal velocities of the particles at these vertices are almost identical. As we move inside the curves, from the vertices, the exiting velocity becomes different from the injecting velocity. Panels (a)–(d) of Fig. 5, respectively, show the time evolution of the radial

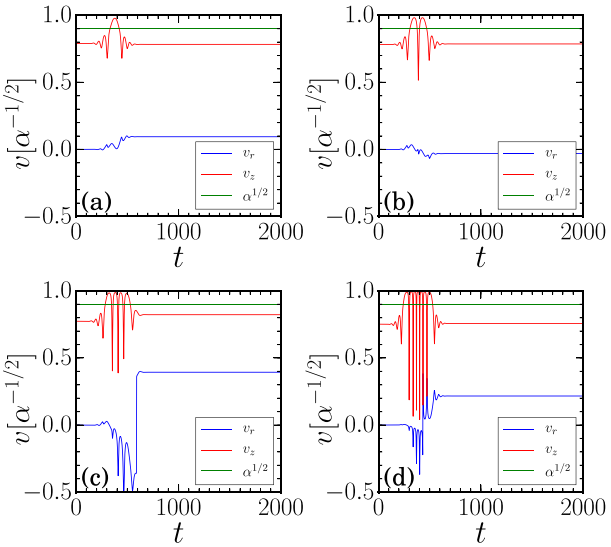

FIG. 5. Panels (a)–(d) show the time evolution of the longitudinal velocity (red solid line) and the radial velocity (blue solid line) of the particle for $\sqrt{\alpha}=0.9$, $\varphi_0=1.0$, $\sigma_z=100$, and $\sigma_r=50$: $r(t=0)=76.59$ and $v_z(t=0)[\alpha^{-1/2}]=0.791$ for panel (a), $r(t=0)=68.86$ and $v_z(t=0)[\alpha^{-1/2}]=0.7824$ for panel (b), $r(t=0)=57.98$ and $v_z(t=0)[\alpha^{-1/2}]=0.7738$ for panel (c), and $r(t=0)=8.8$ and $v_z(t=0)[\alpha^{-1/2}]=0.7544$ for panel (d). This set of parameters is represented by the label 5a, 5b, 5c, and 5d in Fig. 1.

and longitudinal velocities of the particles for the points 5*a*, 5*b*, 5*c*, and 5*d* of Fig. 1. In the panels, we see that if we move downwards and leftwards along a imaginary line that passes through the vertices, the number of oscillations around the resonant line increases by one unit for each half moon passed [one oscillation for panel (a), two for (b), four for (c) and seven for (d)]. The presence of the curves must be related with some resonance that does not let the particle to sustain its peak velocity. This half moon structure is also seen when we plot a colour graded map of the final radial velocity. These curves must be avoided, if we are interested in accelerating and focusing the particle.

In Fig. 6, a color graded map is plotted, where the colors represent the minimum value of the r-coordinate of the particle, normalized by the initial r-coordinate of the particle $-r_{min}/r_0$. The vertical axis is for r_0 and the horizontal one is for $v_{z0}[\alpha^{-1/2}]$. This map, as Fig. 1, was built using $\alpha^{1/2}=0.90$, $\varphi_0=1$, $\sigma_r=50$, and $\sigma_z=100$. The blue color is for minimum values of $r_{min}/r_0\approx 1$, while the black color represents the focusing dynamics and it is for $r_{min}/r_0\approx 0$. When Fig. 6 is compared to Fig. 1 (the white dashed line is the transition between the acceleration regime and the passing and the reflecting regimes), it can be seen that in the accelerating regime, the particle is also focused, except for a narrow region near the white line.

In this small region, during the trapping of the particle (it occurs while z is near 0), the mean value of $\cos(z-t)$ is negative, which implies that the mean of $\partial p_r/\partial t$ is also negative. But as $v_r(t)$ and $r(t)$ are considerably big before the trapping, the negative mean value of the radial acceleration along the time is not enough to focus the particle. If r_0 decreases, then the particle is accelerated and focused as well, as can be seen in the black color region inside the acceleration region of Fig. 6.

Until this point, φ_0 was considered fixed and equal to 1, but this parameter should be in fact explored to give a complete overview of the problem. In Fig. 7, built for $\sqrt{\alpha}=0.9$, $\sigma_z=100$, $\sigma_r=50$, and $r_0=5$, the color graded map indicate

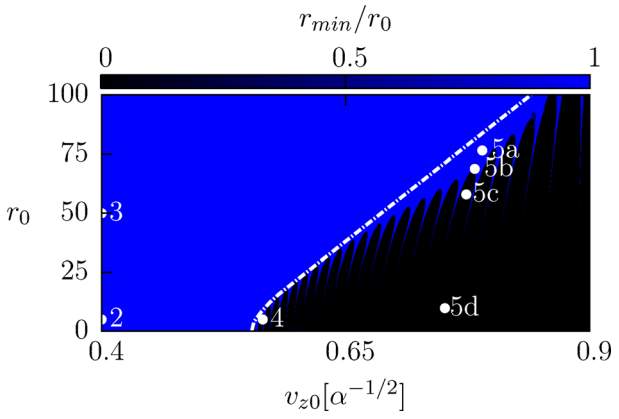

FIG. 6. Color graded map of the minimum value of $r(t)/r_0$ for $\alpha^{1/2}=0.90$, $\varphi_0=1$, $\sigma_r=50$, and $\sigma_z=100$. In the horizontal axis is represented the initial speed of the particle, v_{z0}, while in the vertical axis is expressed r_0. Black (blue) color is for focusing (non-focusing) dynamics. The white dashed line is the transition line seen in Fig. 1 between the acceleration regime and the passing and the reflecting regimes.

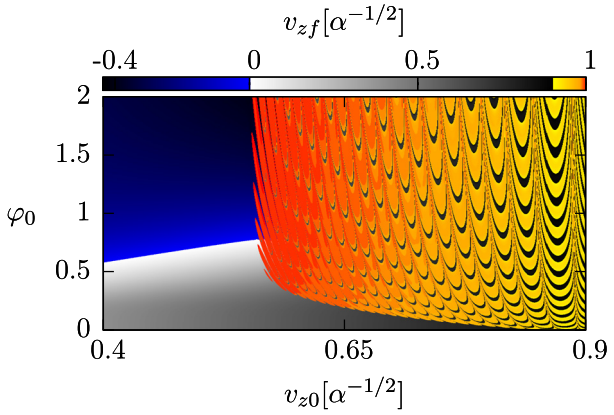

FIG. 7. Color graded map of the longitudinal exiting velocities for $\alpha^{1/2}=0.90$, $r_0=5$, $\sigma_r=50$, and $\sigma_z=100$. In the horizontal axis is represented the initial speed of the particle, v_{z0}, while in the vertical axis is expressed the amplitude of the electrostatic field φ_0. Yellow and red are for velocities greater than $0.90c$.

in the horizontal axis the initial longitudinal velocity of the particle, in the vertical axis the amplitude of the electrostatic wave (φ_0), while the colors represent the exiting velocity of the particle. Three regions may be also identified: the reflecting regime (blue color); the passing regime (gray color); and the accelerating regime (yellow and red colors). The half moon structures are seen as well. The particle's dynamics in each of these regimes are similar in comparison with what is already shown in this work. For very small values of φ_0, the initial longitudinal velocity needed to accelerate the particle is nearest of the resonant velocity than for higher values of φ_0. For values of $\varphi_0>0.4$, the minimum initial longitudinal velocity required to accelerate the particle is about 0.58 and does not depend on φ_0. This kind of structured was observed in Ref. 11.

Finally, α was kept fixed ($\sqrt{\alpha}=0.9$) during this work. As seen in Ref. 11, if we increase the value of the phase-velocity of the carrier, the minimum value of v_{z0} needed to be in the accelerating regime also increases (as well the final velocity). Although the limits of the regions should be modified by changing α, the physics behind the whole process is the same. This way, α, as σ_r and σ_z, could be treated as a scale factor.

IV. CONCLUSION

In this work, a three-dimensional model of an alternative particle accelerator was proposed. The accelerating process is due to a slowly modulated high frequency carrier wave. The field analyzed here has a smoothly varying transverse profile and is slowly modulated along the longitudinal coordinate z. Both the transverse profile and the longitudinal modulation are given by Gaussian functions. Three main regimes were identified with the help of a map of parameters: the reflecting regime, where the particle is reflected by the electrostatic wave; the passing regime, in which the particle passes through the electrostatic wave without significant acceleration/deceleration; and, finally, the accelerating

regime, whose high efficiency is helped by a self-adjusted optimal wave-particle relative phasing.

A ponderomotive approximation (which suppresses the high frequency associated with the longitudinal coordinate) was developed, giving good predictions for the mean value of the radial and longitudinal velocities of the particle. The validity of the approximation is limited to regions far from the accelerating regime. As in Ref. 11, the approximation fails when the maximum of the particle's longitudinal velocity along the particle's dynamics closes to the phase-velocity of the carrier.

The mechanism of acceleration is basically the same as in Ref. 11: when the longitudinal velocity of the particle touches the resonance line, the particle is captured by the electrostatic field and the particle is accelerated towards c. However, one important additional feature of this accelerator is that, under proper conditions, while the particle is accelerated, it is also focused by the field.

Some effects must be added to the model in order to provide more realistic results. Space-charge effects may be relevant if we consider a relatively dense particle beam: The focusing effect seen in the accelerating regime competes against the Coulombian repulsion between the particles. Moreover, a dense particle beam could modify significantly the field intensity: A self-consistent dynamics of the field should be considered then. Furthermore, due to the acceleration gradients of the particles, the problem of radiation reaction must be taken into account.

Owing to its simplicity, the present particle model provides relatively clear directions indicating how to explore this subject of particle acceleration and focusing resulting from the breakdown of the ponderomotive regimes. Further results shall be reported as progress is made.

ACKNOWLEDGMENTS

We acknowledge the support from CNPq and CAPES, Brazil, and from AFOSR, USA, under research Grant No. FA9550-16-1-0280. S.M. acknowledges the support from Grant No. ANR-11-IDEX-0004-02 Plas@Par.

[1]J. D. Cockcroft and E. T. S. Walton, Nature **129**, 649 (1932).
[2]R. J. Van de Graaff, K. T. Compton, and L. C. Van Atta, Phys. Rev. **43**, 149 (1933).
[3]D. W. Kerst, Phys. Rev. **60**, 47 (1941).
[4]R. Bingham, J. T. Mendonça, and P. K. Shukla, Plasma Phys. Controlled Fusion **46**, R1 (2004).
[5]R. Bingham, Philos. Trans. R. Soc. A **366**, 1749 (2008).
[6]C. Kamperidis, C. Bellei, N. Bourgeois, M. C. Kaluza, K. Krushelnick, S. P. D. Mangles, J. R. Marques, S. R. Nagel, and Z. Najmudin, Phys. Plasmas **78**, 433 (2012).
[7]T. P. Hughes and B. Godfrey, Phys. Fluids **29**, 1698 (1986).
[8]A. Steinhof, Nucl. Instrum. Methods Phys. Res. A **397**, 371 (1997).
[9]V. Shiltsev, Y. Alexahin, A. Burov, and A. Valishev, Phys. Rev. Lett. **119**, 134802 (2017).
[10]R. Pakter and F. B. Rizzato, Phys. Rev. E **65**, 056503 (2002).
[11]S. Marini, E. Peter, G. I. de Oliveira, and F. B. Rizzato, Phys. Plasmas **24**, 093113 (2017).
[12]P. K. Shukla, N. N. Rao, M. Y. Yu, and N. L. Tsintsadze, Phys. Rep. **138**, 1 (1986).
[13]J. T. Mendonça, *Theory of Photon Acceleration* (IOP Publishing, Bristol, 2001).
[14]D. Farina and S. V. Bulanov, Phys. Rev. Lett. **86**, 5289 (2001).
[15]R. Bingham, Nature **424**, 258 (2003).
[16]J. R. Cary J R and A. N. Kaufman, Phys. Fluids **24**, 1238 (1981).
[17]C. Grebogi and R. G. Littlejohn, Phys. Fluids **27**, 1996 (1984).
[18]A. van Steenbergen, J. Gallardo, J. Sandweiss, and J.-M. Fang, Phys. Rev. Lett. **77**, 2690 (1996).
[19]L. F. Monteiro, A. Serbeto, K. H. Tsui, J. T. Mendonça, and R. M. O. Galvão, Phys. Plasmas **20**, 073101 (2013).
[20]E. Peter, A. Endler, and F. B. Rizzato, Phys. Plasmas **21**, 113104 (2014).
[21]P. Mulser and D. Bauer, *High-Power Laser-Matter Interaction* (Springer-Verlag, Berlin, 2010).